ELSEVIER

Journal of Nuclear Materials 297 (2001) 14–26

journal of nuclear materials

www.elsevier.com/locate/jnucmat

# Texture dependent plastic behavior of Zr 702 at large strain

O. Castelnau [a,*], H. Francillette [b], B. Bacroix [a], R.A. Lebensohn [c]

[a] *Institut Galilée, LPMTM-CNRS, Université Paris-Nord, av. J.B. Clément, Villetaneuse 93430, France*
[b] *GRCM, INSA, 20 av. des Buttes de coemes, Rennes 35043, France*
[c] *Instituto de Física Rosario (UNR-CONICET), 27 de Febrero 210bis, Rosario 2000, Argentine*

Received 12 December 2000; accepted 18 April 2001

**Abstract**

Three polycrystalline samples of Zr702α are deformed at room temperature under channel die compression until about 40% strain. Samples are oriented differently in the die with respect to their texture, so that the influence of the initial texture on the stress–strain response, the activated deformation systems, and the subsequent texture evolution can be assessed. Experimental results are interpreted by using a viscoplastic self-consistent (VPSC) polycrystalline model in which a saturating anisotropic intracrystalline hardening law is introduced. It is shown that the orientation dependence of the activated slip systems strongly depends on the texture of the polycrystal. The main effect of intracrystalline hardening is found to be a redistribution of slip from the primary to the secondary systems, but in a moderate way such that it does not affect significantly the development of texture. A simple analysis shows that the increasing activity of the secondary slip systems can be assessed directly from the macroscopic stress–strain curves. 

## 1. Introduction

The difficulty of understanding the plastic behavior of zirconium alloys is mainly due to the fact that, owing to the hexagonal symmetry of the lattice cell, less than 5 independent 'easy glide' slip systems (the so-called primary systems) are available. That is, for accommodating any arbitrary deformation, hard glide systems (the secondary systems) should be activated [1]. The critical resolved shear stress (CRSS) of the primary systems can be relatively easily determined experimentally by deformation tests on single crystals [2,3]. Due to the elongated shape of the single crystal yield surface [4], it is more difficult to perform proper mechanical tests for which only secondary systems are activated. On the other hand, the CRSS determined on single crystals are not necessarily relevant for polycrystal plasticity owing to effects of grain size, grain boundaries, etc. [5]. The ratio between the CRSS of secondary and primary systems are generally found or assumed to lie between 1.2 and 15, see for example [6–9]. The significant width of this interval clearly reveals the difficulty to assess a precise determination of the critical stress of the hard systems. At room temperature, zirconium polycrystals deform essentially by dislocation glide on $\{10\bar{1}0\}\langle 11\bar{2}0\rangle$ prismatic systems (which provide only two independent slip systems) and by $\{10\bar{1}2\}$, $\{11\bar{2}1\}$, and $\{11\bar{2}2\}$ twinning [10–12]. Concerning secondary slip systems, many experimental studies have shown the occurrence of first-order pyramidal slips $\{10\bar{1}1\}\langle 11\bar{2}0\rangle$ and $\{10\bar{1}1\}\langle\bar{2}113\rangle$ [10], the latter allowing a crystal reduction along the $\langle c\rangle$ axis. Several independent works have also proved the possible activation of basal slip $\{0001\}\langle 11\bar{2}0\rangle$ [8,13,14]. Consequently, axial deformation along the *c*-axis is rather hard unless twinning systems are activated, whereas axial deformation perpendicular to this axis is easily produced by prismatic glide. This property renders the deformation rate highly dependent on the crystallographic orientation of grains in the polycrystal, leading also to a strong local interaction between the grains and their neighbors. At large strains, the evolution of intracrystalline hardening, crystallographic texture, and macroscopic plastic

* Corresponding author. Tel.: +33-1 49 40 34 68; fax: +33-1 49 40 39 38.
*E-mail address:* oc@lpmtm.univ-paris13.fr (O. Castelnau).

0022-3115/01/$ - see front matter 
PII: S0022-3115(01)00589-X

behavior are closely related since they are all the result of dislocation glide. Hardening mechanisms are quite well characterized in cubic single crystals since only a few well identified slip families contribute to the deformation [15,16]. In these materials, they were found to have a significant influence on texture development [17–19]. In hexagonal materials like zirconium, the experimental characterization of intracrystalline hardening becomes a very difficult task because several not well-defined secondary slip systems may be active simultaneously. Its influence on texture development and macroscopic behavior is not clear at present.

Owing to the large plastic anisotropy of single crystals, a significant influence of texture on the plastic behavior is observed, e.g., see [9]. In previous work, Francillette and coworkers [8,20–22] have deformed several specimens of zirconium 702 under channel die compression, so that the influence of the initial texture on subsequent texture evolution, slip system activation, and macroscopic behavior could be partially studied. The aim of the present work is to go deeper into the analysis by applying a polycrystal deformation model inferred from homogenization. It is worth pointing out that the use of such a physical based model is satisfactory only if the model correctly describes (at least) the contribution of each slip system to the total deformation, and particularly a realistic activity for the secondary systems. In several works published recently, the static model (uniform stress), the Taylor model (uniform strain rate), or an heuristic approach close to the Taylor bound are applied to low symmetry crystals such as zirconium, see for example [6–8,14,23]. The uniform stress lower bound completely neglects intergranular internal stresses, whereas the uniform strain rate upper bound overestimates grain interactions and thus gives rise to a too high contribution of the secondary slip systems [1,24–26]. Here, we use the tangent formulation of the viscoplastic self-consistent (VPSC) model [27,28] which captures more accurately the main features of polycrystal plasticity, i.e., a concentration of dislocation glide in the primary systems together with strong intergranular interactions. This model has already been applied to zirconium alloys, e.g., see [5,28,29]. More recently [9,30], intracrystalline hardening was introduced into the model using relatively simple hardening law, and only a rapid comparison to experiment was performed. Here, we apply the viscoplastic self-consistent model to assess the influence of intracrystalline hardening on (i) the activation of the different slip systems with respect to the crystallographic orientation, (ii) the evolution of the crystallographic texture, and (iii) the macroscopic behavior. The parameters of the hardening law are identified on the bulk experimental response of the specimens, and we verify each time that model results are consistent with the experiments at both microscopic and macroscopic scales.

## 2. Experimental results

Channel die compression tests up to about 40% strain have been performed at room temperature on three Zr-702 polycrystalline samples exhibiting similar chemical composition and microstructure, but different initial crystallographic textures. Further details on the experimental procedure and results can be found in [8,20–22]; only an outline is given here. Tests were carried out with a constant cross-head speed corresponding to a normal strain rate of about $10^{-4}$ $s^{-1}$, and a thin Teflon film was inserted between the sample surfaces and the apparatus platen to avoid any friction [31]. Before testing, all samples were annealed at 450°C for 3 h.

Initial textures are shown in Fig. 1(a), where the direction '1' denotes the longitudinal direction (LD) of the channel die, '2' denotes the transverse direction (TD), and '3' the normal direction (ND). The texture of sample T1 corresponds to the classical rolling texture, T3 is obtained by cross-rolling, and T4 is a 90° rotation of T3 around LD. Deformation textures measured after about 40% normal deformation are shown in Fig. 1(b). As compared to the initial textures, basal poles in T1 are slightly closer to ND and slightly spread in the LD–TD plane, while no significant evolution of prismatic poles is observed. T4 presents a slight reorientation of basal poles around ND with a significant alignment of prismatic pole along LD. T3 exhibits a particular behavior, with almost no texture evolution.

Fig. 2 shows the macroscopic mechanical behavior of the three samples. Since we are interested only in the large strain plastic regime, the first 2% of deformation, which corresponds to the elastic–viscoplastic transition are not presented here. For T4, the normal stress increases almost linearly with strain after about 5% strain, whereas the stress–strain curve has a more curved shape for T3. T1 exhibits an intermediate behavior. Note that the strength of all samples is very different. For example after 20% deformation, the flow stress of T3 is about twice that of T4.

The active slip systems have been identified with a scanning electronic microscope at 20% strain. The technique consists in (i) measuring the crystallographic orientation of the grain, (ii) measuring the orientation of the slip trace(s) at the same position (the slip trace is the intersection of a slip plane with the free surface of the specimen), and (iii) identifying the possible activated slip system. Table 1 indicates the number of grains in which prismatic, pyramidal or basal slip traces are identified. Due to the small grain size, the slip traces of a given grain can be observed only on one free surface of the specimen; therefore, the corresponding activated slip system sometimes cannot be completely determined. These ambiguous cases are also indicated in Table 1. For T4, prismatic slip is largely dominant, and few traces of pyramidal slip are identified. For T1, a globally similar

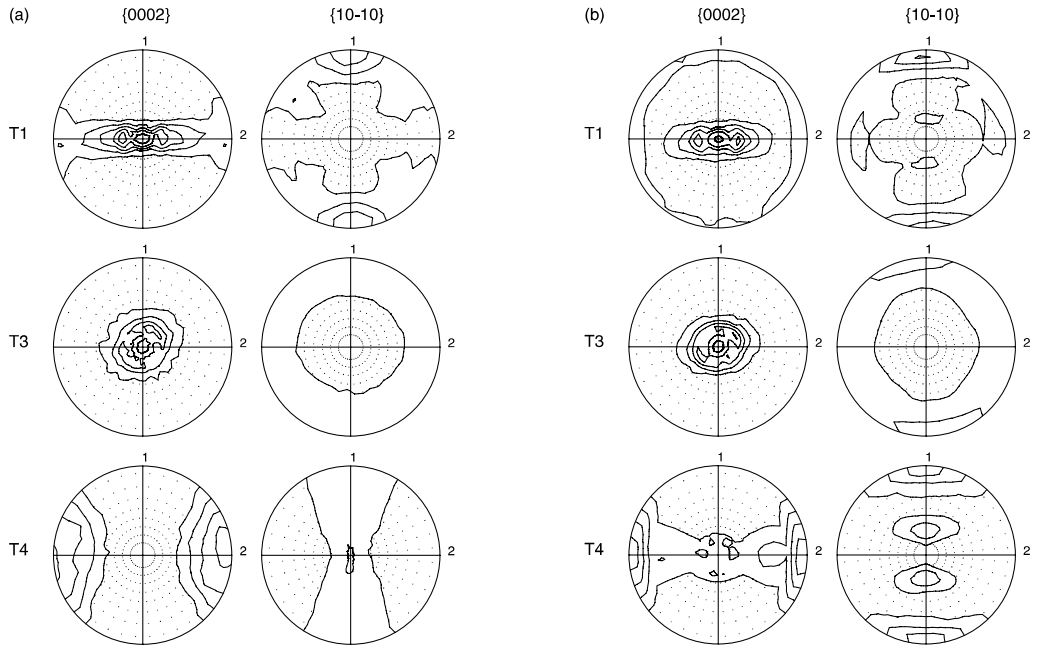


Fig. 1. Experimental textures of T1, T3, and T4 specimens: (a) initial states; (b) after 40% plane strain, 1 = LD, 2 = TD, 3 = ND. Levels = 1, 2, 3, ... (× random intensity).

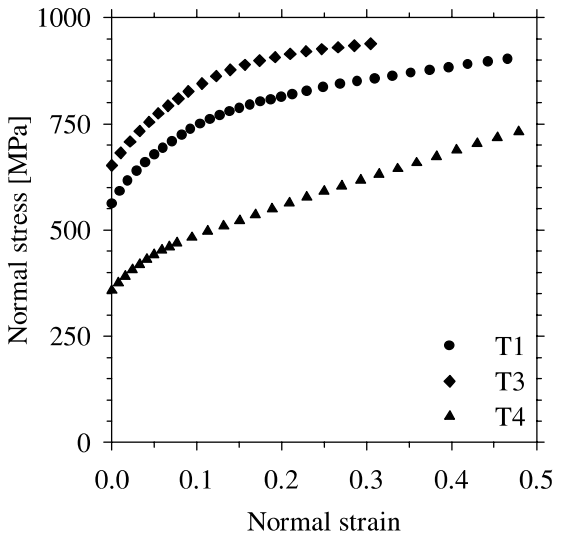


Fig. 2. Experimental plastic response of T1, T3, and T4 specimens.

behavior is found, however with more ambiguity between prismatic and pyramidal slips. For T3, the activity of pyramidal slip is significant. Basal slip could have occurred to a small amount in T1 and T3, but the identification of the basal plane as slip plane is always ambiguous for these samples. However, traces close to the basal plane have been observed unambiguously in two other samples (not presented here because of the large activity of twinning) of the same initial zirconium sheets loaded in different directions, indicating that basal slip must be considered as a potentially active secondary mechanism [21,22]. Table 1 also indicates the surface twinned fraction (STF) at 20% axial strain. Here, only tensile twining $\{10\bar{1}2\}\langle\bar{1}011\rangle$ is observed. The highest twinned fraction (about 5%) is found for T4.

Consequently, T3 and T4 exhibit 'opposite' behaviors, T1 being intermediate. T4 presents a large texture development, the lowest stress level, and the largest activity of prismatic slip, whereas T3 exhibits almost no texture development, the highest stress level, and a significant activity of pyramidal slip.

Table 1
Sample, number of grains (in %) in which prismatic (pr.), pyramidal (pyr.), and basal (ba.) slip are observed, and STF in %[a]

| Sample | Pr. | Pyr. | Pr. or pyr. | Pyr. or ba. | Pr. or pyr. or ba. | STF |
|---|---|---|---|---|---|---|
| T1 | 30 | 0 | 65 | 0 | 5 | 2.0 |
| T3 | 37 | 17 | 33 | 7 | 7 | 2.3 |
| T4 | 61 | 2 | 37 | 0 | 0 | 5.2 |

[a] Measurements were performed at 20% strain on 40, 30, and 51 grains for T1, T3, and T4, respectively. From [31].

## 3. Local behavior and homogenization scheme

### 3.1. The polycrystalline model

For analyzing the experimental data, we use the 'tangent' formulation of the VPSC model developed in a general framework by Molinari et al. [27] and applied to anisotropic materials by Lebensohn and Tomé [28]. The self-consistent (SC) scheme allows the calculation of the average mechanical quantities (stress and strain rate) in each 'phase' of the material (a *phase* denotes the set of all grains that have the same lattice orientation). Basically, the SC scheme consists in modeling the interaction between all the grains of a phase with their surrounding by the interaction between an ellipsoidal inhomogeneity with the same lattice orientation than the phase embedded in an infinite homogeneous equivalent medium (HEM) whose behavior describes that of the polycrystal. The related inclusion problem is solved by an extension of the classical Eshelby formalism [32] to viscoplastic materials. To do so, the local constitutive relation needs to be linearized with respect to the local stress, and, within the VPSC model, the linearized behavior is also used to relate the average strain rate of a phase to the corresponding average stress. The advantages of the self-consistent scheme is that it allows average stress and strain rate to be different in each grain depending on the lattice orientation, and calculations can be performed with less than five independent slip systems in each grain [33].

Recently, more accurate homogenization procedures have been developed for viscoplastic polycrystals, namely the 'affine model' [34], the 'second-order procedure' [35], and the 'variational estimates' [36]. The main difference between these models is essentially related to the method used for the linearization of the local behavior and to the application of this linearized behavior to local average stress and strain rate. Although these methods are theoretically more accurate than the VPSC model, they have never been applied up to now to large deformation of polycrystals, so that their use is out of the scope of the present work. Furthermore, they predict a relatively stiff response of the material (except for the second-order procedure) and for this point of view, the VPSC model is generally closer to reality (but with a less consistent formulation). A limitation of the VPSC model is that it violates a new restrictive upper bound [37] under specific circumstances (as does also the affine model, but not the variational estimates). However, even if not perfect, the VPSC model captures the most important features for zirconium plasticity, i.e., a dominant activation of the soft slip systems, strong intergranular interactions, and texture evolution.

### 3.2. Deformation mechanisms

To the authors' knowledge, three different schemes have been developed so far to incorporate deformation twinning in polycrystal plasticity models. In these approaches, the twinned region of a grain is either treated as a new grain – no difference is then made between the new twin and an old deformed grain – [38,39] or it is assumed to deform identically as the untwinned region of the grain – invoking thus the Taylor model – [40]. Furthermore, it is not clear how twin and slip mechanisms interact, so that one can hardly at present treat twinning and intracrystalline hardening simultaneously in polycrystal models. As shown in Section 2, the twinned fractions are very small in our samples. Note that this is not the case generally; in the present case, the small twinning activity is directly linked to the texture of the material and to the small grain size (15–20 μm). As a first approximation, one can therefore consider that twinning has a negligible influence on texture development. Furthermore, it can be verified numerically that the strength of twinning very poorly influences the flow stress level of T1, T3, and T4. Consequently, twinning can be neglected here. According to experimental observations, the deformation mechanisms taken into account are prismatic $\{10\bar{1}0\}\langle 11\bar{2}0\rangle$, pyramidal $\{10\bar{1}1\}\langle 11\bar{2}3\rangle$, and basal $\{0001\}\langle 11\bar{2}0\rangle$ slip. Pyramidal $\langle a\rangle$ was initially also taken into account, but its activity was always found to be negligible. The reason for that is that this slip system is geometrically not very different than the softer prismatic slip. For this reason, pyramidal $\langle a\rangle$ is not considered anymore in the following. The considered local constitutive relation is a classical power law. The shear rate $\dot{\gamma}^s$ on the slip systems $s$ is expressed by [41]

$$\dot{\gamma}^s = \dot{\gamma}_0 \left| \frac{\tau_r^s}{\tau_0^s} \right|^{n-1} \frac{\tau_r^s}{\tau_0^s}, \tag{1}$$

where $\dot{\gamma}_0$ is a reference shear rate taken here equal to unity ($\dot{\gamma}_0 = 1\ \mathrm{s}^{-1}$), and $\tau_r^s$ is the resolved shear stress on the system $s$. The stress exponent $n$ and the CRSS $\tau_0^s$ are the parameters of this constitutive relation. The CRSS may vary with strain owing to intracrystalline hardening, as it will be discussed later. A stress sensitivity $n = 19$ is taken for all slip systems. This value is close enough to the experimental value ($n \approx 30$, [42]) to avoid significant errors in numerical results, but it is small enough to avoid the VPSC model to tend to the lower uniform stress bound as observed for higher stress sensitivities [28]. Initial textures consist in a set of 1944 orientations, with associated volume fractions derived from the pole figure measurements.

### 3.3. Boundary conditions

A special attention has been paid to the prescribed macroscopic boundary conditions in order to reproduce as closely as possible a real channel die compression test. This is particularly important owing to the significant anisotropy of samples. Usually, calculations are performed with a prescribed strain rate tensor of the form: $\overline{D}_{12} = \overline{D}_{13} = \overline{D}_{23} = 0$, and initial textures are assumed to exhibit an ideally orthotropic symmetry. According to Canova et al. [43], the macroscopic stress takes a similar form in that case: $\overline{S}_{12} = \overline{S}_{13} = \overline{S}_{23} = 0$. Here, calculations are performed with experimental textures which are approximately – but not exactly – orthotropic and therefore no particular symmetry is assumed a priori. We account for the fact that the surface normal to LD is stress free and that no shear strain occurs in the ND–TD plane. The macroscopic velocity gradient and deviatoric stress finally read

$$\overline{\mathbf{L}} = \begin{bmatrix} \overline{L}_{11} & \overline{L}_{12} & \overline{L}_{13} \\ 0 & 0 & 0 \\ 0 & 0 & \overline{L}_{33} \end{bmatrix} \quad \text{and} \quad \overline{\mathbf{S}} = \begin{bmatrix} \overline{S}_{11} & 0 & 0 \\ 0 & \overline{S}_{22} & \overline{S}_{23} \\ 0 & \overline{S}_{32} & \overline{S}_{33} \end{bmatrix} \tag{2}$$

with $|\overline{L}_{33}|$ increasing with strain to reproduce the constant cross-head speed.

## 4. Analysis of initial stress levels

The difficulty of using a micro–macro model to understand the plastic behavior of zirconium polycrystals is that several parameters must be identified. In this section, we first omit intracrystalline hardening to concentrate on the initiation of slip and in particular on the influence of initial prismatic, pyramidal, and basal CRSS ($\tau_0^{pr}, \tau_0^{pyr}, \tau_0^{ba}$) on the macroscopic behavior of polycrystals. The global procedure used here consists in determining a first set of parameters for which the model well reproduces the three initial macroscopic flow stresses. Results will be interpreted in terms of the dependence of slip system activity on the crystallographic orientation.

It is possible to calculate with the VPSC model for various values of $\tau_0^{pyr}/\tau_0^{pr}$ and $\tau_0^{ba}/\tau_0^{pr}$, the flow stress of T1, T3, and T4 corresponding to the initial texture, i.e., to the first deformation step. Results are shown in Fig. 3, where the stress of T1 and T3 is normalized by that of T4 for the sake of clarity. Experimental values of the initial flow stress are 560 MPa for T1, 650 MPa for T3, and 360 MPa for T4, that is experiments correspond to the isovalue levels 1.57 for T1 ($= \sigma^{T1}/\sigma^{T4}$) and 1.82 for T3 ($= \sigma^{T3}/\sigma^{T4}$) as shown with dotted lines in Figs. 3(a) and (b), respectively. A careful comparison of these figures shows that both isolines are almost superimposed. This means that, if one considers only the macroscopic compliance, several set of CRSS lead to acceptable results. One could think using additional mechanical tests to determine more precisely the CRSS. But this procedure is not straightforward since other orientations of sample with respect to the prescribed deformation generally lead to an non-negligible activity of twinning systems.

According to Fig. 4, the prismatic activity of each sample keeps an almost constant value within this whole set of solution for the three samples. One can therefore favor either pyramidal or basal glide with neither consequence on the prismatic activity nor on the initial macroscopic flow stress. A simulation with conditions favoring basal glide leads to texture development in good agreement with experiments. However, the activity of pyramidal systems is found to be insignificant and basal activity is too large for T3 (more than 20%), in

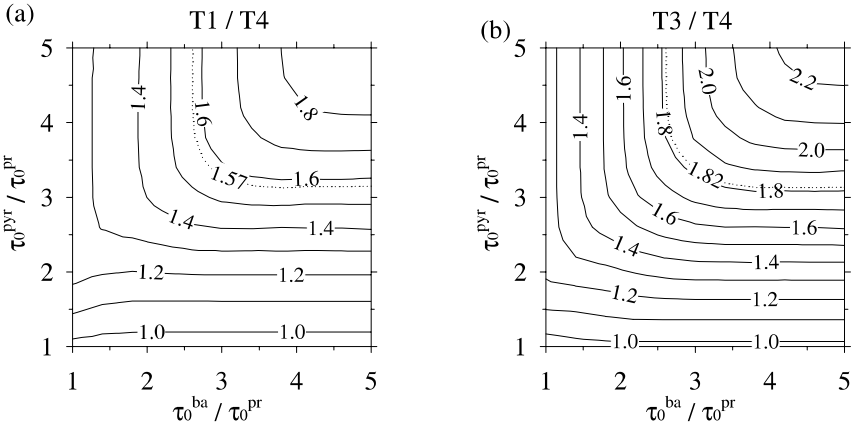


Fig. 3. Isovalues of the ratio between normal stresses at the first step of deformation: (a) $\sigma^{T1}/\sigma^{T4}$; (b) $\sigma^{T3}/\sigma^{T4}$, calculated as a function of $\tau_0^{pyr}/\tau_0^{pr}$ and $\tau_0^{ba}/\tau_0^{pr}$.

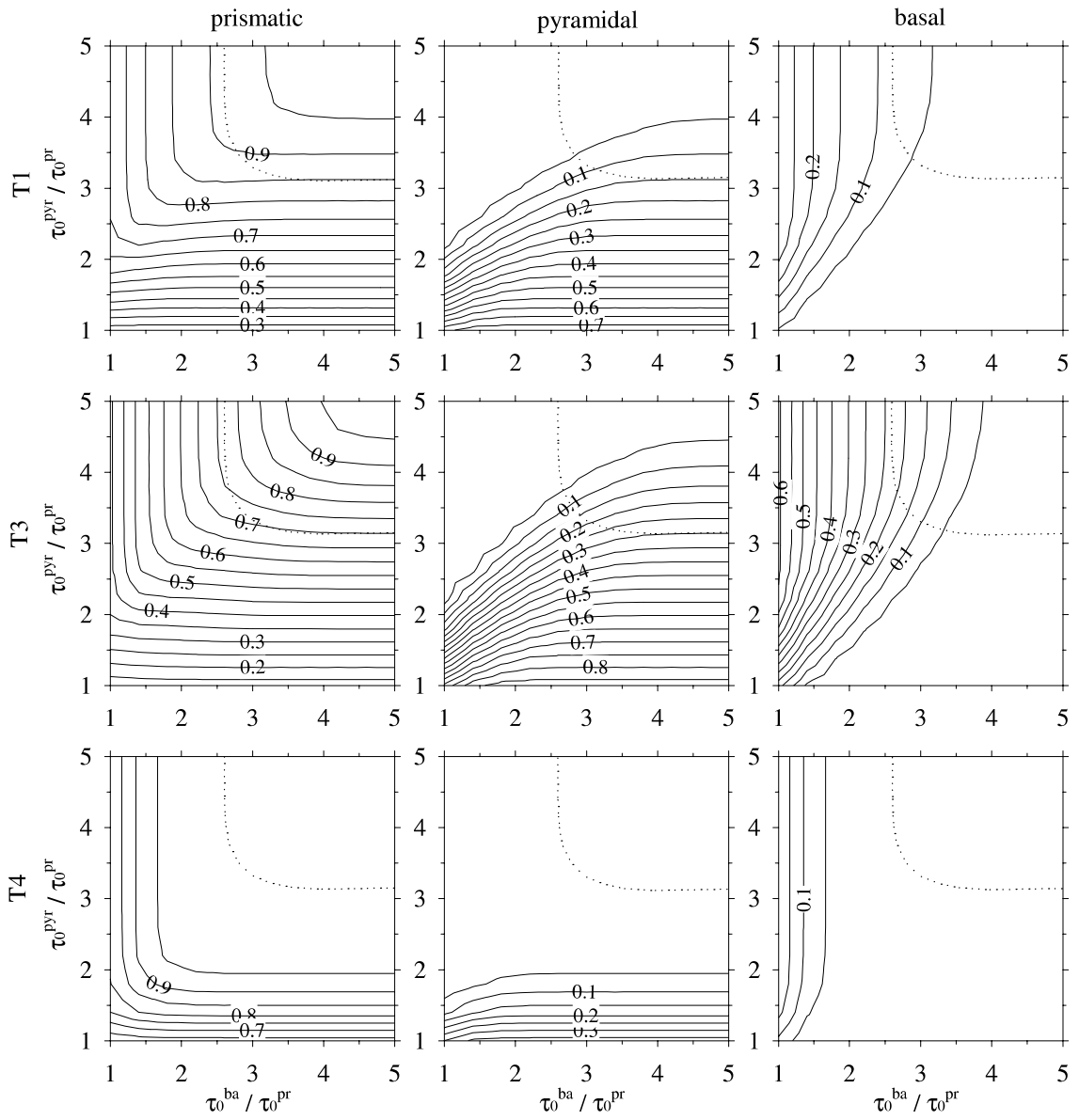


Fig. 4. Isovalues of the slip system activities calculated for T1, T3, and T4 as a function of $\tau_0^{pyr}/\tau_0^{pr}$ and $\tau_0^{ba}/\tau_0^{pr}$. The dotted line shows the possible CRSS ratios.

disagreement with Table 1. On the other hand, for conditions favoring pyramidal slip, the {0 0 0 2} pole figure of T1 and T3 exhibit a very low intensity along ND. This discrepancy is not observed when basal glide is activated. Consequently, texture development and slip system activities can be best reproduced simultaneously only if $\tau_0^{pyr}$ and $\tau_0^{ba}$ have approximately the same value. Thus, even if in the present case, a complete agreement between experimental and predicted textures is not expected since hardening is not taken into account yet, we choose the following initial values for the CRSS:

$$\tau_0^{pyr} = \tau_0^{ba} = 3.2\tau_0^{pr}, \tag{3}$$

with $\tau_0^{pr} = 164$ MPa to reproduce the stress level of T4. This value for the prismatic CRSS compares well with those obtained by other authors on other zirconium specimens [7,23,28,44].

The complete calculated behavior (texture development, stress–strain curves, slip system activities) of T1, T3, and T4 specimens is shown in Fig. 5 for this set of parameters. The textures simulated after 40% strain are globally similar to the experimental ones, however again

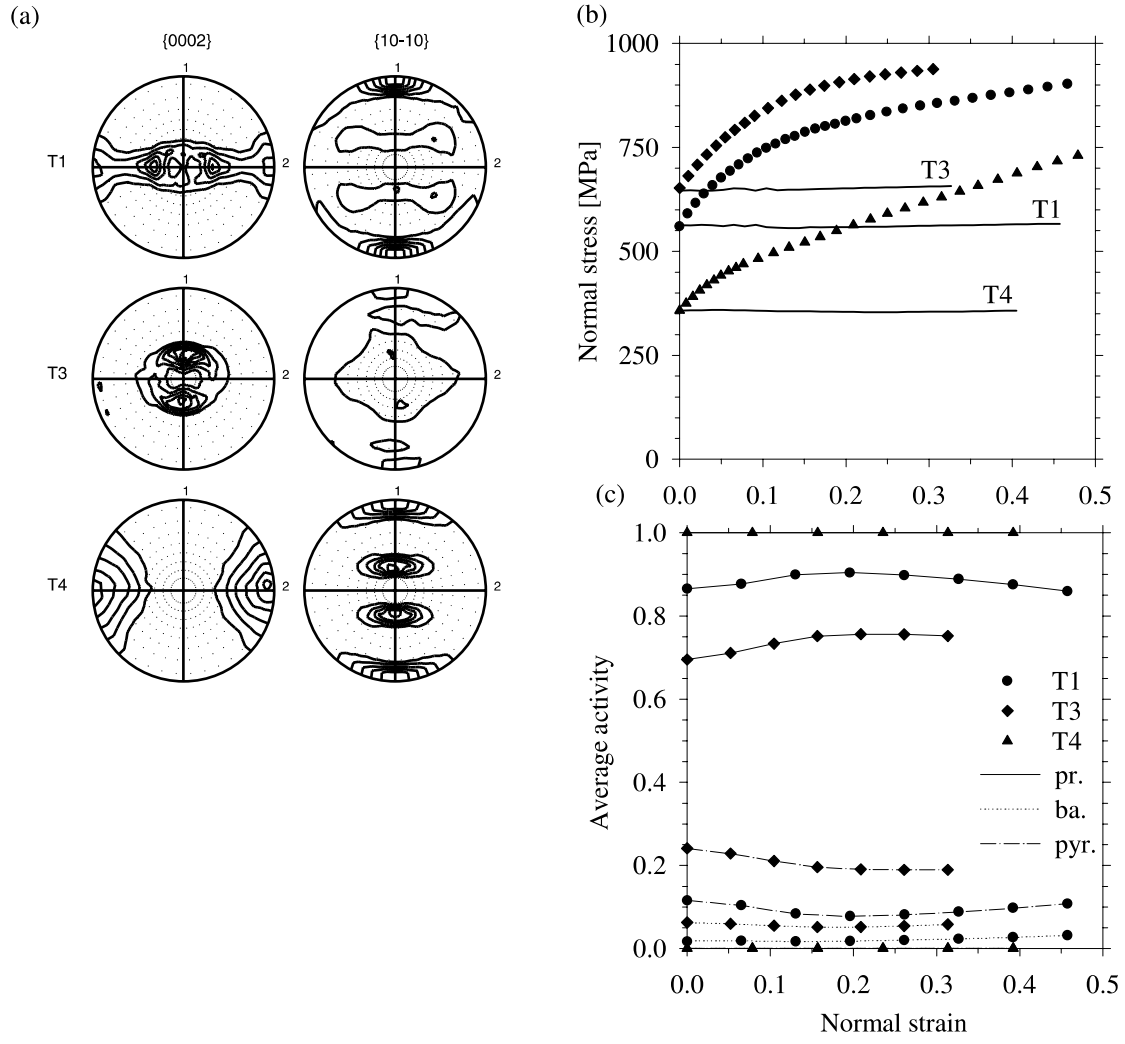


Fig. 5. Prediction obtained without hardening for $\tau_0^{pyr} = \tau_0^{ba} = 3.2\tau_0^{pr}$, and $\tau_0^{pr} = 164$ MPa: (a) textures after 40% strain (levels $= 1, 2, 3, \ldots \times$ random intensity); (b) comparison of simulated macroscopic behaviors (lines) with experimental data (dots); (c) relative activity of prismatic, pyramidal, and basal slip families.

with a too small intensity of $\{0\,0\,0\,2\}$ poles along ND for T3. Slip system activities are approximately independent on strain (Fig. 5(c)). T4 deforms only by prismatic glide. For T3, the relative contribution of pyramidal slip to the total deformation is about 20%, and that of basal slip about 7%. The activity of secondary systems is lower for T1 than for T3. Globally, the activities are thus consistent with experiments, see Table 1, which means also that basal slip cannot be increased much to improve the texture development of T3. In Fig. 5(b), we see that the three initial flow stresses are very well reproduced. However, all stress–strain curves are surprisingly flat, indicating that geometrical hardening is insignificant, even for T4 where the texture development is rather large. Therefore, the experimental hardening of the three samples can be fully attributed to intracrystalline hardening. The question now is to understand how intracrystalline hardening affects texture development. This point is investigated in the following section.

## 5. Influence of intracrystalline hardening on the plastic behavior

### 5.1. Intracrystalline hardening law

Very few publications deal with hardening laws for hexagonal materials and, to our opinion, no attempt was really satisfactorily. In [30], strain hardening is introduced in a self-consistent model but in a quite simple

and unrealistic way since only self-hardening is considered. In [9], the hardening of prismatic and $\langle c+a \rangle$ pyramidal slip is assumed to be described by a Voce type law, but the identification of parameters on two macroscopic stress–strain responses leads to an unrealistically small activation of prismatic slip (30%). In [14], a more elaborated 'physical based' hardening law is considered, but the author uses a homogenization scheme that significantly underestimates strain heterogenity (hard grains deform almost as much as soft grains) [45], so that the physical relevance of the identified local parameters can hardly be interpreted; for example, the dislocation densities are found to be approximately equal on primary and secondary systems, in disagreement with TEM observations.

From the stress–strain curve of T3, it is clear that the hardening law should be able to reproduce a decreasing hardening rate with increasing strain for an almost constant texture. It should also be able to reproduce the different shapes of the macroscopic stress–strain curves as observed experimentally. Furthermore, due to the complex geometry of slip systems, self- and latent-hardening should behave differently [46]. On the other hand, for the sake of simplicity, the hardening law should not contain a too large number of parameters to be determined. A first attempt to use a hardening law with a constant hardening matrix was performed, and almost linear stress–strain curves were obtained, in disagreement with experiments. Therefore, we choose the anisotropic law proposed by Bronkhorst et al. [47], which captures in a simple way the main hardening features, i.e., saturation of the CRSS and anisotropy. A similar expression was also used in [45]. The CRSS evolution rate reads

$$\dot{\tau}_0^s = \sum_l H_{sl} \left| \dot{\gamma}^l \right|, \tag{4}$$

where the components of the hardening matrix $H$ are given by the following expression:

$$H_{sl} = H_0 \left( 1 - \frac{\tau_0^l}{\tau_{\text{sat}}^l} \right)^a Q_{sl} \tag{5}$$

with

$$Q_{sl} = \begin{cases} 1 & \text{if } s = l, \\ Q_0 & \text{otherwise.} \end{cases} \tag{6}$$

The term $Q_{sl}$ allows to account for a smoother self- ($Q_{ss}$) than latent- ($Q_{sl}, s \neq l$) hardening, $\tau_{\text{sat}}^s$ is a saturation stress, and the coefficient $H_0$ and the exponent $a$ describe the average hardening rate. Therefore, apart from the initial values of the CRSS of the three slip families, six additional parameters ($\tau_{\text{sat}}^{\text{pr}}, \tau_{\text{sat}}^{\text{pyr}}, \tau_{\text{sat}}^{\text{ba}}, a, H_0, Q_0$) must be calculated by the identification process in order to characterize the selected hardening law. It is worth noting that the VPSC model allows the grains to deform differently from each other and therefore a different hardening matrix must be calculated for each grain at each deformation increment. Consequently, the macroscopic hardening is generally not isotropic even when intracrystalline hardening reduces to Taylor-type isotropic hardening ($a = 0,\ Q_0 = 1$). It will be shown in the next section that some results are qualitatively independent on the particular form of this hardening law.

### 5.2. Effect of hardening on the plastic behavior

Results are plotted in Fig. 6. It is worth pointing out that the identification problem has not a unique solution, i.e., several sets of parameters lead to very similar simulated stress–strain curves, texture development, and slip system activities. The coefficients corresponding to the best fit are indicated in Table 2. They have been obtained using an optimization code especially designed to derive quantitative hardening parameters from experimental data by the way of a standard minimization procedure. As in Section 4, parameters are identified here on the macroscopic stress–strain curves. For T4, a good reproduction of the experimental macroscopic stress–strain curves is obtained. For T3, however, the asymptotic shape of the experimental curve is not very well described. It is not clear at present why it is so: the polycrystalline model, the shape of the hardening law, or the too small amount of experimental data could be increminated. This is currently under investigation. According to Fig. 6(a), intracrystalline hardening has only a small influence on texture development, and slightly better results were obtained without hardening. Indeed, the intensity of $\{0\,0\,0\,2\}$ poles along ND is much smaller than expected for both T1 and T3. Intracrystalline hardening therefore does not improve texture prediction at all. As compared to Fig. 5(c), slip system activity is now clearly evolving with strain. It is in good agreement with experiments for the softer sample (T4), for which secondary systems very poorly contribute to the deformation. For T3 and T1, the large number of ambiguously determined slip traces (see Table 1) makes the comparison more difficult, but experimental and simulated activities are not contradictory. Therefore, intracrystalline hardening mainly increases the stress level by increasing the activity of secondary systems, this without any improvement of the predicted texture.

## 6. Discussion

The deformation of three samples, exhibiting almost identical initial textures, for different orientation in the channel die clearly highlights the large texture dependent macroscopic plastic anisotropy of Zr polycrystals. Two samples present somehow an 'opposite' behavior, T4 (significant texture development, low stress level,

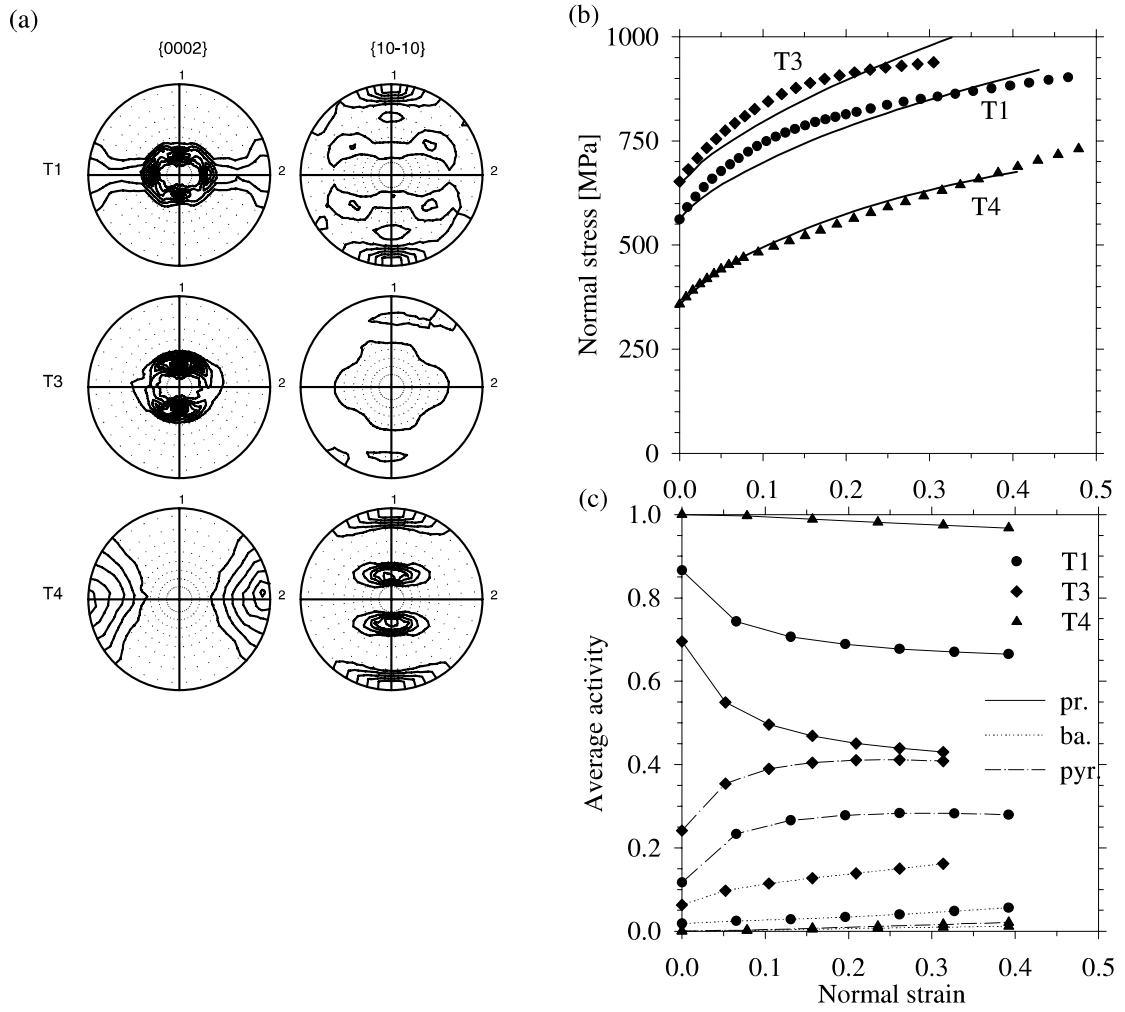


Fig. 6. Predictions obtained with intracrystalline hardening for the three samples: (a) textures after 40% normal strain (levels $= 1, 2, 3, \ldots \times$ random intensity); (b) calculated normal stresses (lines) as compared to experiments (dots); (c) relative activity of prismatic, pyramidal, and basal slip families.

Table 2
Values of the initial CRSSs and the parameters of the hardening law[a]

| | Pr. | Pyr. | Ba. |
|---|---|---|---|
| $\tau_0$ (MPa) | 164 | 525 | 525 |
| $\tau_{sat}$ (MPa) | 410 | 1280 | 1220 |
| | $H_0 = 777$ MPa | $Q_0 = 1.47$ | $a = 1.91$ |

[a] Note that $\tau_0/\tau_{sat} \approx 0.4$ for each slip family.

large activity of the primary slip system) and T3 (almost no texture development, high stress level, significant activity of secondary slip systems), the third sample T1 being always intermediate. We will therefore mainly discuss the behavior of T3 and T4. Due to the small grain size and the texture orientation in the channel die, twinning is almost not activated, so that it can soundly be neglected. The experiments are interpreted using a VPSC model, where the CRSSs and their subsequent evolutions with strain have been identified to reproduce the macroscopic mechanical responses. Globally, the flow stress levels and texture development are well reproduced numerically, whereas a slightly better agreement is obtained for T4. As compared to bcc materials [17,18], intracrystalline hardening has here very little influence on texture development. Indeed, for the three investigated specimens, prismatic glide always remains the most active system. This is particularly true for T4 for which other slip systems are almost not activated.

In the initial texture of T4, grains are mainly oriented with the $\langle c \rangle$ axis approximately parallel to TD. They are thus mainly subjected to axial deformations perpendicular to the $\langle c \rangle$ axis, which can be fully accommodated by prismatic glide. For channel die compression and spherical grains, the plastic rotation rate is the leading term for texture development. It corresponds to a rotation around an axis parallel to the slip plane and normal to the Burgers vector. Consequently, the large prismatic activity of T4 essentially leads to a reorientation of the $\{1\,0\,\bar{1}\,0\}$ poles. The slight reorientation of $\{0\,0\,0\,2\}$ poles observed experimentally (Fig. 1) can thus be attributed to second-order features such as intergranular interaction, slip on secondary systems, grain shape, etc. The situation of T3 is more complicated. One cannot describe this sample as if it would consist of a single orientation with $\langle c \rangle$ axis parallel to ND since in that case only pyramidal glide would be activated. Concerning the evolution of the $\{0\,0\,0\,2\}$ pole figure, pyramidal and basal slips have opposite effects; the former reorients $\{0\,0\,0\,2\}$ poles along LD while the latter reorients them along ND. The very small texture evolution of T3 can therefore only be explained by a selected combination of the activity of both slip systems.

A feature found here is that the activity of the secondary systems significantly increases with strain for both T1 and T3. This was also obtained with other hardening laws, so this result seems to be general and not dependent on the particular form of Eq. (5). In fact, it can be shown that the increasing activity of the secondary systems is directly linked to the form of the macroscopic stress–strain curves. According to Fig. 7, the flow stress of T4 is almost insensitive to the CRSS of the secondary systems for CRSS ratios larger than 2. In a first approximation, one can therefore conclude that the flow stress of T4 is directly proportional to the CRSS of prismatic glide only. According to Fig. 2, $\tau_0^{pr}$ thus increases by a factor 1.55 between 0% and 20% strain. More slip systems are activated in T3 than in T4 owing to the texture which favors the secondary systems. With a larger latent- than self-hardening, $\tau_0^{pr}$ for T3 should thus increases by a factor of at least 1.55 between 0% and 20% strain. That is, for this sample, pyramidal and basal glides would keep a constant activity with strain only if both $\tau_0^{pyr}$ and $\tau_0^{ba}$ increase to a same amount as $\tau_0^{pr}$, i.e., a factor 1.55. In that case, the macroscopic flow stress of T3 would become at 20% strain as high as 1010 MPa instead of 910 MPa as observed experimentally. Secondary slip systems thus necessarily harden less than the primary system, relatively to their initial CRSS value. As shown in Fig. 8, the net increase $\Delta\tau_0$ of the CRSS is very similar for the prismatic, pyramidal, and basal systems, but the ratio $\tau_0^{pyr,ba}/\tau_0^{pr}$ decreases with strain as also found in [9]. That is, even with a quite larger latent- than self-hardening ($Q_0 = 1.47$), prismatic slip remains by far the softest slip system. Note that this feature is directly linked to the relatively large value ($\simeq 3.2$) of the ratio $\tau_0^{pyr,ba}/\tau_0^{pr}$ at the beginning of the deformation. The main effect of hardening is a redistribution of slip from primary to secondary systems, but in a moderate way such that its effect on texture development is not significant. This is particularly the case for T4 for which prismatic glide remains by far the most active system. Concerning texture evolution in T1 and T3, a worse agreement with experiment is obtained when hardening is taken into account in the model, the main difference being a too small intensity of the $\{0\,0\,0\,2\}$ poles along ND. This feature can be directly attributed to larger increase of the pyramidal slip as compared to basal slip. One way to avoid this effect would be to take into account tensile twinning observed (to a very small amount) experimentally. According to Francillette [31], the twinned parts of grains have $\langle c \rangle$ axes approximately parallel to ND. But it is not clear at present how

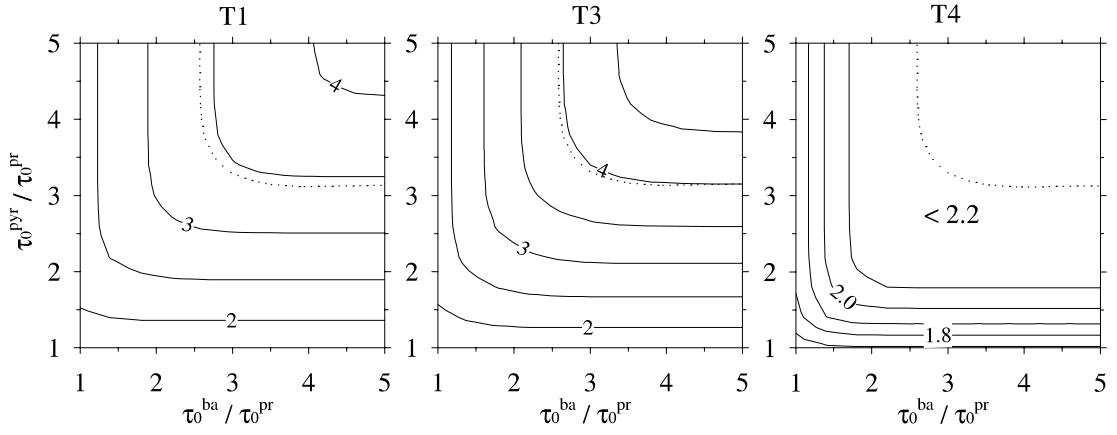


Fig. 7. Relative initial flow stresses $\sigma/\tau_0^{pr}$ as a function of $\tau_0^{pyr}/\tau_0^{pr}$ and $\tau_0^{ba}/\tau_0^{pr}$ for T1, T3, and T4. The dotted line shows the possible CRSS ratios.

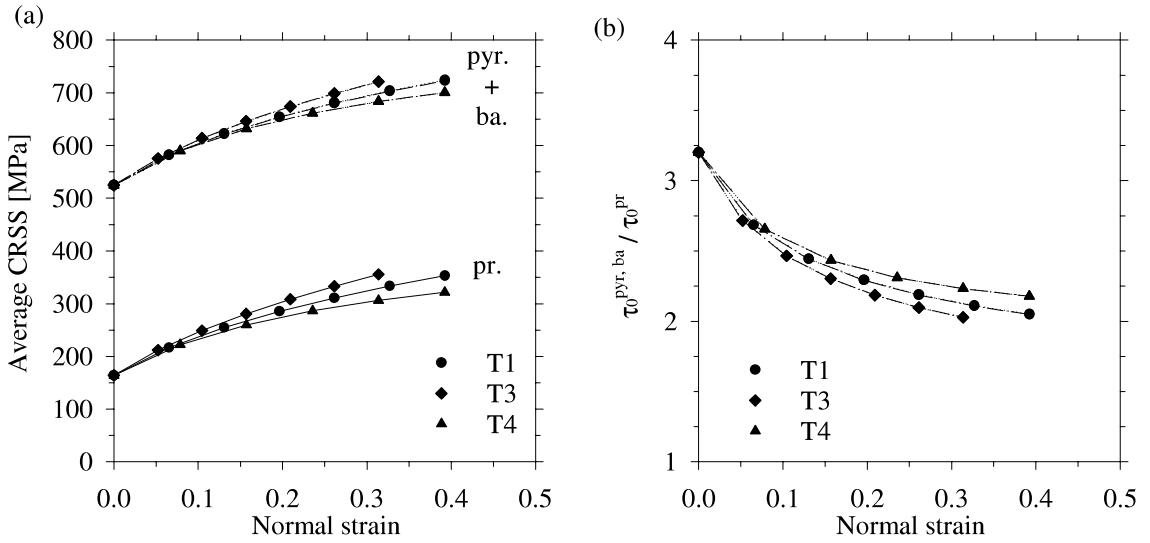


Fig. 8. Predicted evolution with strain of: (a) the prismatic, pyramidal, and basal CRSS for T1, T3, and T4; (b) the ratio $\tau_0^{pyr,ba}/\tau_0^{pr}$ between CRSS of secondary and primary slip systems.

twinning and hardening can be treated simultaneously as discussed before, and this problem is beyond the scope of this work.

So far, we have verified that the distribution of dislocation glide on the primary and secondary slip systems is well reproduced in *average* for the whole polycrystal. A more local analysis is presented in Fig. 9, which shows the activated slip systems for each crystallographic orientation and each sample, as predicted by the model and compared to experiments. The third Euler angle $\varphi_2$ (rotation around the $\langle c \rangle$ axis) is not considered here since its influence is small. It appears clearly that, for a given lattice orientation, the activation of a particular slip system is not only dependent on the lattice orientation, but also strongly depends on the texture of the polycrystal. This is because the interaction between each phase with the rest of the material depends on the overall behavior of the polycrystal. From Fig. 9, the agreement of T4 with experiment is very good. Recall that, for this specimen, very good results were also found for texture development and stress–strain curve. T4 appears thus as a sample quite 'easy' to reproduce numerically, and it is so because (i) the prescribed deformation largely favors prismatic slip in all phases and (ii) all phases have approximately the same lattice orientation, so that the contrast (in terms of rheology) between the phases is small. For T1 and T3, results of Fig. 9 are globally consistent with experiments, but the comparison is not as straightforward as for T4 because of the large number of ambiguous cases between prismatic and pyramidal slip. One should also keep in mind that the VPSC model gives only quantities (here activities) averaged over a whole phase, whereas experiments provide informations concerning individual grains, i.e., concerning a small part of the phase. However, it seems more probable from Fig. 9 that these ambiguous cases correspond to prismatic slip in agreement with expectations based on TEM observations. For T3, the result concerning basal slip is of particular interest. Indeed, it is found that the grains in which basal slip could have occured (ambiguous cases) correspond effectively to orientation where basal slip is predicted, showing that the activation of basal slip is mostly probable.

## 7. Conclusion

Texture development, macroscopic mechanical response, and activity of slip systems were studied experimentally for the three samples of zirconium 702 with different orientations of the initial texture. Two samples can be distinguished by their 'opposite' behavior: T4 exhibits a large texture development, a low stress level, and a large activity of prismatic slip, whereas T3 exhibits almost no texture development, a high stress level, and a significant activity of pyramidal slip. Sample T1 is intermediate between T3 and T4. Experiments are interpreted using a VPSC model. This model is believed to capture the main feature of polycrystal plasticity, i.e., the orientation dependence of the activation of the different slip systems. Prismatic, pyramidal $\langle c + a \rangle$, and basal slips were taken into account in the numerical calculations, whereas tensile twinning could be soundly neglected since it was found to be poorly active experimentally. It is shown that geometrical hardening is insignificant for all samples, even for T4 for which the

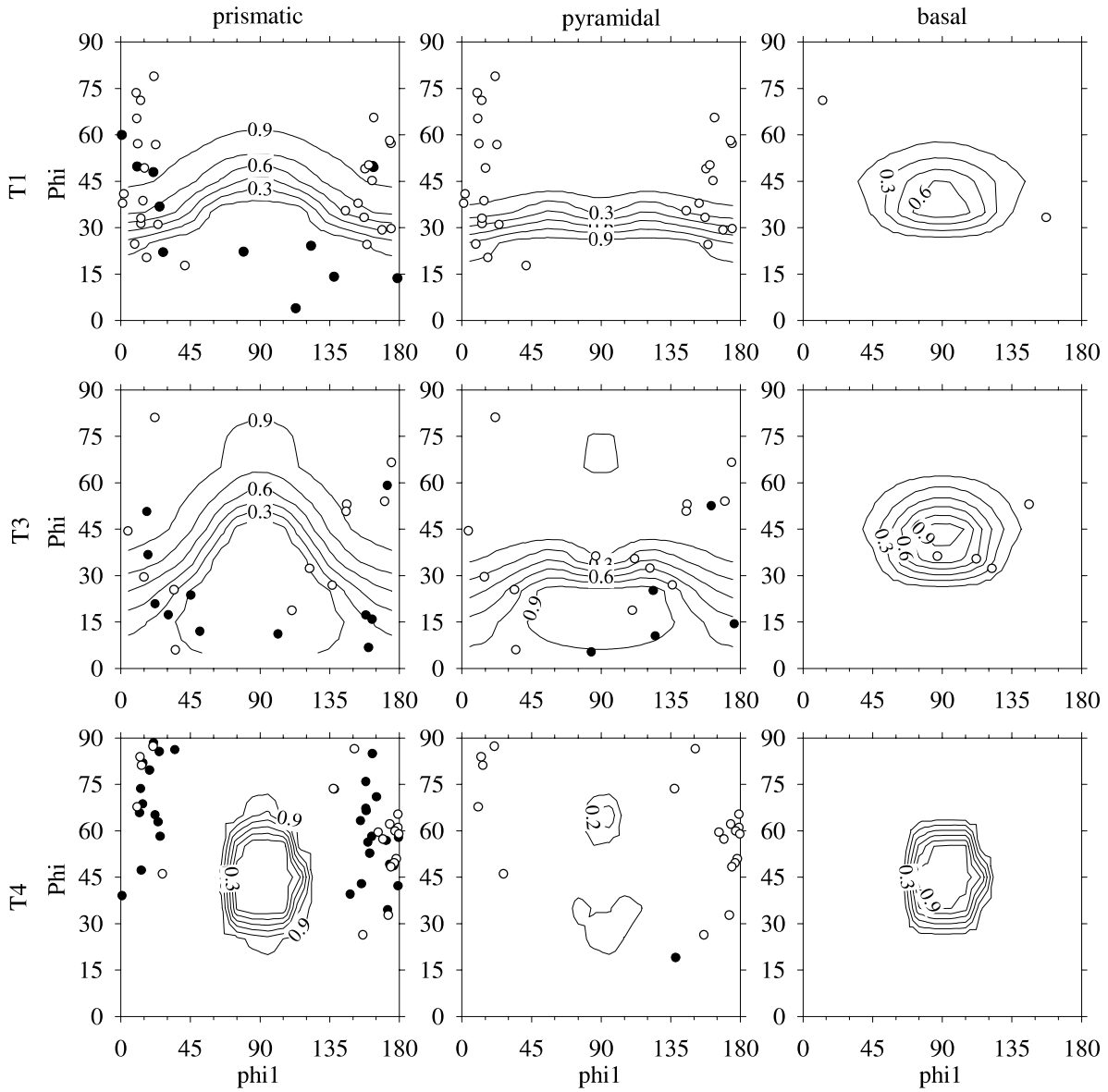


Fig. 9. Relative activity of prismatic, pyramidal, and basal slips predicted with the VPSC model (isolines) as compared to experiments for T1, T3, and T4 (dots). Open circles are used for ambiguously determined traces of slip planes and are thus plotted at least twice (e.g., prismatic and pyramidal). $\varphi_1$ and $\phi$ are the Euler angles of the lattice cell with respect to channel die (Bunge convention). It is worth noting that the experimental points only indicate the occurence of an activity of a given system but does not indicate, as the prediction does, the percentage of activity. The non-uniform repartition of experimental points reflects the textures of the samples.

texture development is rather large. The increase of the applied stress during the deformation can thus fully be attributed to intracrystalline hardening. The orientation dependence of the slip system activity is found to be strongly influenced by the texture. The relative CRSSs of primary and secondary systems are determined according to the three mechanical responses, using a simple anisotropic and saturating hardening law. Globally, all model results (texture development, slip system activities, mechanical response) are in agreement with experiments. Independently on the form of the hardening law used here, it is shown that the activity of the secondary systems necessarily increases with strain for a proper reproduction of the macroscopic stress–strain curves, even with a stronger latent- than self-hardening. However, prismatic slip remains always the dominant deformation process. The main effect of hardening is a redistribution of slip from primary to secondary

systems, but in a moderate way such that it does not affect significantly the development of textures. For sample T4, intracrystalline hardening has really no influence on the texture, since secondary systems are almost inactive also at large strain. For T1 and T3, it is shown that the increasing activity of pyramidal slip leads to a too low intensity of $\{0\,0\,0\,2\}$ poles along ND as compared to experiments. This could be avoided only if tensile twinning $\{1\,0\,\bar{1}\,2\}\langle\bar{1}\,0\,1\,1\rangle$ is taken into account, but this requires further investigations concerning the interaction between twin and slip mechanisms.

## Acknowledgements

The experimental part of this work was partially supported by the Commissariat à l'Energie Atomique. The authors are very grateful to Jean-Luc Béchade, Rénald Brenner, and Monique Gaspérini for fruitful discussions.

## References

[1] U.F. Kocks, Metall. Trans. 1 (1970) 1121.
[2] A. Akhtar, Metall. Trans. A 6 (1975) 1217.
[3] A. Akhtar, E. Teghtsoonian, Acta Metall. 19 (1971) 655.
[4] C. Tomé, U.F. Kocks, Acta Metall. 33 (4) (1985) 603.
[5] A. Salinas-Rodriguez, Acta Metall. Mater. 43 (2) (1995) 485.
[6] J.J. Fundenberger, M.J. Philippe, F. Wagner, C. Esling, Acta Mater. 45 (10) (1997) 4041.
[7] S. Caré, PhD thesis, Ecole Polytechnique, France, 1995.
[8] H. Francillette, B. Bacroix, M. Gasperini, J.L. Béchade, Acta Mater. 46 (12) (1998) 4131.
[9] P.J. Maudlin, C.N. Tomé, G.C. Kaschner, G.T. Gray, in: Sixth International Conference on Numerical Methods in Industrial Forming Processes, University of Twente, Enschede, The Netherlands, 22–25 June, 1998.
[10] A. Akhtar, J. Nucl. Mater. 47 (1973) 79.
[11] R.G. Ballinger, G. Lucas, R. Pelloux, J. Nucl. Mater. 126 (1984) 53.
[12] L. Xiao, H. Gu, Metal. Mater. Trans. A 28 (1997) 1021.
[13] J.L. Martin, R.E. Reed-Hill, Trans. TMS AIME 230 (1964) 780.
[14] P. Geyer, PhD thesis, Ecole Nationale Supérieure des Mines de Paris, France, 1999.
[15] P. Franciosi, Acta Metall. 33 (9) (1985) 1601.
[16] A. Mécif, B. Bacroix, P. Franciosi, Acta Mater. 45 (1) (1997) 371.
[17] T.S. Tóth, in: Z. Liang, L. Zuo, Y. Chu (Eds.), ICOTOM 11, International Academic Publisher, Xi'an, China, 1996, p. 347.
[18] S. Mercier, L.S. Tóth, A. Molinari, Textures Microstruct. 25 (1995) 45.
[19] M. Miller, P. Dawson, J. Mech. Phys. Solids 45 (1997) 1781.
[20] H. Francillette, B. Bacroix, M. Gasperini, O. Castelnau, R.A. Lebensohn, Etude des mécanismes de déformation et des évolutions de textures du zirconium 702 deformé en compression plane à la température ambiante, La Revue de Metallurgie – CIT/Science et Genie des Materiaux, 1997, p. 1071.
[21] H. Francillette, B. Bacroix, M. Gaspérini, J. Béchade, Mater. Sci. Eng. A 234–236 (1997) 974.
[22] H. Francillette, O. Castelnau, B. Bacroix, J.L. Béchade, Mater. Sci. Forum 273–275 (1998) 523.
[23] J. Crépin, T. Bretheau, D. Caldemaison, Acta Metall. Mater. 43 (10) (1995) 3709.
[24] B.J. Lee, S. Ahzi, R.J. Asaro, Mech. Mater. 20 (1995) 1.
[25] O. Castelnau, G.R. Canova, R.A. Lebensohn, P. Duval, Acta Mater. 45 (11) (1997) 4823.
[26] V.C. Prantil, P.R. Dawson, Y.B. Chastel, Modell. Simul. Mater. Sci. Eng. 3 (1995) 215.
[27] A. Molinari, G.R. Canova, S. Ahzi, Acta Metall. 35 (12) (1987) 2983.
[28] R.A. Lebensohn, C.N. Tomé, Acta Metall. 41 (9) (1993) 2611.
[29] R.A. Lebensohn, C.N. Tomé, Mater. Sci. Eng. A 175 (1994) 71.
[30] A.A. Pochettino, P. Sanchez, in: Proceedings of the International Conference on Texture of Materials 12, Montreal, Canada, 9–13 August, 1999.
[31] H. Francillette, PhD thesis, Université Paris-Nord, France, 1997.
[32] J.D. Eshelby, Proc. R. Soc. Lond. A 241 (1957) 376.
[33] J.W. Hutchinson, Metall. Trans. A 8 (9) (1977) 1465.
[34] R. Masson, M. Bornert, P. Suquet, A. Zaoui, J. Mech. Phys. Solids 48 (6–7) (2000) 1203.
[35] M. Bornert, P.P. Castaneda, Proc. R. Soc. Lond. A 454 (1998) 3035.
[36] P. Gilormini, M.V. Nebozhyn, P.P. Castaneda, Acta Mater. 49 (2001) 329.
[37] P. Gilormini, in: Proceedings of the IUTAM Symposium on Micromechanics of Plasticity and Damage of Multiphase Materials, Kluwer Academic, Sèvres (France), August 29–September 1, 1995.
[38] P.V. Houtte, Acta Metall. 26 (1978) 591.
[39] C.N. Tomé, R.A. Lebensohn, U.F. Kocks, Acta Metall. Mater. 39 (11) (1991) 2667.
[40] S.R. Kalidindi, J. Mech. Phys. Solids 46 (2) (1998) 267.
[41] J.W. Hutchinson, Proc. R. Soc. Lond. A 348 (1976) 101.
[42] C. Pujol, PhD thesis, Ecole Nationale Supérieure des Mines de Paris, France, 1994.
[43] G.R. Canova, U.F. Kocks, C.N. Tomé, J.J. Jonas, J. Mech. Phys. Solids 33 (4) (1985) 371.
[44] P.A. Turner, N. Christodoulou, C.N. Tomé, Int. J. Plasticity. 11 (3) (1995) 251.
[45] R. Brenner, PhD thesis, Université Paris Nord, France, 2001.
[46] G.J. Weng, Int. J. Plasticity. 3 (1987) 315.
[47] C.A. Bronkhorst, S.R. Kalidindi, L. Anand, Proc. R. Soc. Lond. A 341 (1992) 443.